Design of On-Chip Compatible Concurrent Dual Band Millimeter Wave Antenna

Smriti Agarwal*

Abstract—This paper presents the design and analysis of an on-chip compatible millimeter wave (mm-wave) antenna concurrently operating at frequencies 60 GHz and 94 GHz. It is quite challenging to design an antenna at mm-wave frequency due to propagation of surface waves and use of high index Si substrate for system on-chip (SoC) applications. Hence, in this paper a micromachined mm-wave antenna design using suspended microstrip technology has been proposed for SoC applications. Dual band operation of the antenna has been achieved by reactive loading at the radiating edge. The designed antenna supports the fractional bandwidth of 3.7% & 5% and gain of 7.68 dBi & 8.22 dBi at 60 GHz and 94 GHz, respectively. The results were also compared using two different EM solvers HFSS and CST which were in close agreement. Parametric effects of different substrate and antenna design parameters have also been analyzed. As a proof of concept, a scaled prototype antenna was fabricated and compared with the proposed mm-wave antenna.

1. INTRODUCTION

Millimeter wave (mm-wave) frequency is gaining enormous interest nowadays due to the growing demand of high data rate communications and limitations of over flooded traffic at microwave frequency [1–3]. The use of mm-wave frequency provides compact, handheld systems at affordable cost for various applications including wireless local area networks (WLAN), wireless personal area network (WPAN), sensing, imaging, and vehicular communication [4–7]. CMOS based system on-chip (SoC) technology requires integration of an antenna on a single high index substrate (*viz.* Si, GaAs, InP); therefore, planar antennas are the preferred choice. However, at mm-wave the performance of planar antennas on these high index substrates ($\varepsilon_r = 10$–13) greatly decreases due to surface wave propagation losses. This leads to reduction in bandwidth and radiation efficiency of the antenna [8]. Further, the conductivity of a semiconductor substrate also leads to losses and causes degradation in antenna performance. To meet the SoC integration requirements and to simultaneously achieve optimized antenna performance on high index substrates, different techniques have been proposed by various researchers. A solution to achieve efficient antenna performance for on chip application is to locally create a low effective index region beneath and around the antenna. This can be achieved through different techniques, e.g., bulk micromachining, where wafer is selectively anisotropically etched [9–13]; surface micromachining in which microstructure is built by deposition and etching of different layers in steps; photonic band gap (PBG) materials where closely spaced holes are drilled to perturb the formation of surface wave modes [14–16] and by elevating the patch radiator [17]. In all such cases, the overall approach is to somehow reduce the effective dielectric constant of the substrate used in the designing of antenna.

Moreover, nowadays the use of dual-band antennas at mm-wave frequency is gaining interest among researchers due to simultaneous support to multiple applications and added redundancy. Some of the

reported antennas are: 60/77 GHz fractal bowtie antenna using movable plate [18], split ring resonator (SRR) based antenna for 40/60 GHz band [19], and 24/60 GHz antenna using 0.13-μm standard CMOS process [20]. However, micromachining based dual-band mm-wave antenna technique has still not been investigated although it could have great potential to compensate losses at mm-wave frequency. Therefore, a dual-band (60 GHz and 94 GHz) antenna using micromachined technology on a silicon substrate has been proposed having high gain and bandwidth for SoC applications. The paper is divided into following sections. Section 2 of the paper deals with the design of dual-band mm-wave antenna design concept. Section 3 deals with the results and discussion of suspended microstrip line and dual-band antenna. As a proof of concept, measured characteristics of the scaled fabricated prototype are discussed in Section 4. Finally, Section 5 covers conclusion.

2. MM-WAVE DUAL BAND ANTENNA DESIGN APPROACH

2.1. Challenges in mm-Wave Antenna Design

For mm-wave MMIC applications, antennas require essential features like 1) Compact and light weight, 2) easy integration for RF front end applications, 3) high efficiency and bandwidth. Keeping in view of these prerequisites, micromachining technique for the antenna design has been chosen which lowers the effective dielectric constant and facilitates better antenna performance even on high index silicon. Thereby, introduction of an air cavity beneath antenna inhibits surface wave and other higher order mode propagation and hence reduces losses [11, 21].

Further at mm-wave, antenna dimensions are very small ($\lambda/2 \approx 1.5$ to 2.5 mm) due to correspondingly much lower wavelengths. Hence, commonly practiced dual-band antenna techniques at microwave frequencies, like vertically stacked patches, cutting slots within patch, closely spaced parasitic patches, cannot be directly applied with feasible accuracy and precision at mm-wave [22]. Therefore, it is quite challenging to keep the antenna design simple as well as achieving optimal performance for dual-band antenna operation.

2.2. Suspended Microstrip Line Technology for MMIC

Figure 1(a) shows the geometry of suspended microstrip line on a high index silicon wafer. Due to unavailability of empirical formulae for suspended microstrip technology, different characteristic features of the suspended microstrip line *viz.* effective dielectric constant and characteristic impedance w.r.t.
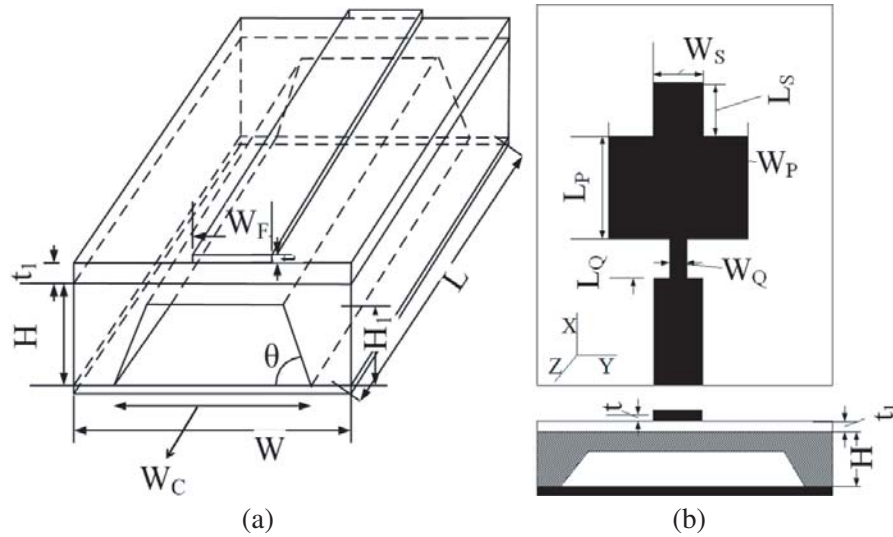

(a)   (b)

Figure 1. Geometry of (a) suspended microstrip line and, (b) dual band mm-wave antenna on the bulk micromachined silicon substrate.

frequency were obtained by parameterization of air cavity height using 3D EM solver HFSS (FEM based). The detailed characterization process of suspended microstrip line is discussed in Section 3. These characteristic parameters will be utilized in the estimation of width of different suspended microstrip line sections, i.e., microstrip feed ($50\,\Omega$) and matching network.

2.3. Proposed Dual Band Antenna Design

Figure 1(b) demonstrates the design of the mm-wave dual-band antenna on micromachined Si wafer. The proposed antenna geometry consists of an initial radiating patch fed by a $50\,\Omega$ suspended microstrip line through a quarter wave matching network. Instead of coax feeding, inline microstrip feeding has been preferred in view of fabrication constraints of feeding at mm-wave frequency. Further, for exciting dual resonances, either a $\lambda/4$ open or $\lambda/2$ short stub was thought to be placed at the radiating edge of main patch [23]. However, due to complexities in shorting the stub to the ground, an open circuit stub has been used. Input impedance of a stub will be capacitive or inductive depending upon the stub length, neglecting transmission line losses. This approach provides reactive loading to the basic main patch. Input impedance (Z_{oc}) of open circuit stub is [23]

$$Z_{oc} = -jZ_0 \cot(\beta l) \tag{1}$$

where l = length of stub, β = propagation constant, Z_0 = characteristic impedance of stub.

At $\beta l = (2\Pi/\lambda) \times (\lambda/4) = \Pi/2$, the stub will show resonant behaviour and hence will provide the second resonant frequency needed for dual-band operation of antenna. Thus, the overall structure of proposed mm-wave antenna will maintain low profile characteristic while simultaneously providing dual frequency operation with excellent inter-band rejection capability. Further, Fig. 2 depicts a flowchart showing different steps for the design of a dual frequency micromachined mm-wave antenna for MMIC applications.
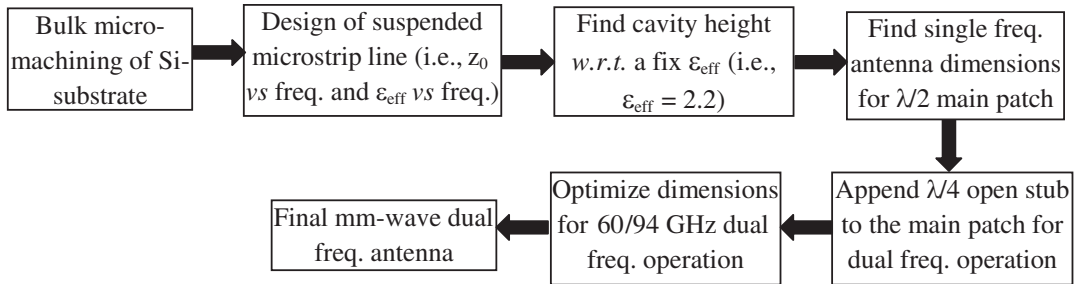

Figure 2. Flow chart showing steps for the design of dual frequency mm-wave antenna using bulk micromachining for MMIC applications.

3. RESULTS AND DISCUSSION

A high resistivity Silicon wafer substrate ($\varepsilon_r = 11.7$, thickness $H = 0.254\,\text{mm}$, resistivity $\rho = 5000\,\Omega$-cm) with an oxide layer of SiO_2 ($\varepsilon_r = 4$, and thickness $t_1 = 0.002\,\text{mm}$) was considered in view of MMIC applications for the proposed dual-band antenna simulation. For metallization, Gold coating with thickness $t = 0.002\,\text{mm}$ and conductivity $\sigma = 4.1 \times 10^7\,\text{S/m}$ has been used. The size of the Si wafer was ($L \times W$) $10\,\text{mm} \times 10\,\text{mm}$. Extensive EM wave simulations have been carried out using two commercially available 3D full wave EM solvers HFSS and CST MWS in order to compare the performance.

3.1. Characterization of mm-Wave Suspended Microstrip Line

An air cavity has been created between silicon substrate and ground plane using bulk micromachining ($\theta = 54.74°$) in order to implement suspended microstrip technology. Depending upon the air cavity height (H_1), the effective dielectric constant (ε_{eff}) of silicon wafer will vary from 11.7 to nearly 1
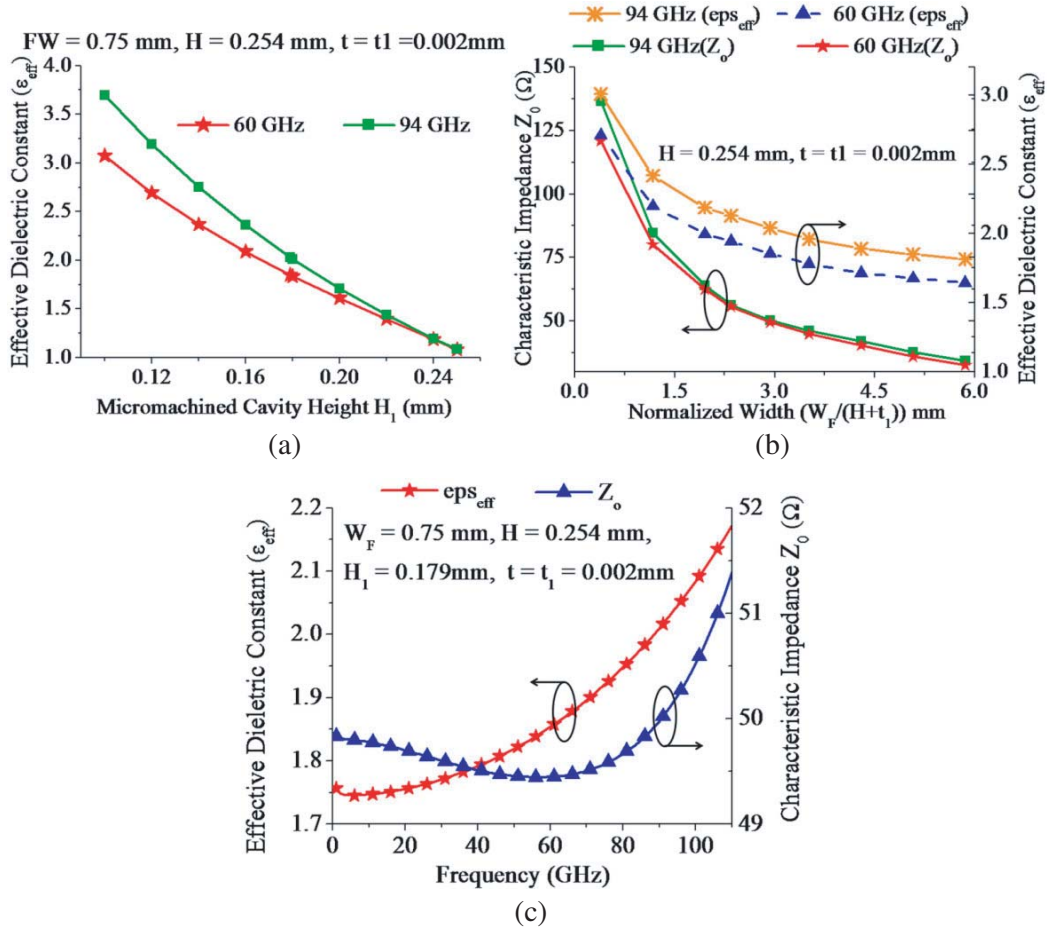
Figure 3. Characterization of suspended microstrip line at millimeter wave. (a) ε_{eff} vs cavity height, (b) ε_{eff} and Z_0 vs normalized conductor width, (c) ε_{eff} and Z_0 vs frequency.

(one) [24]. The variation in ε_{eff} with respect to cavity height, for fixed conductor width (W_F) is shown in Fig. 3(a) at both 60 GHz and 94 GHz. As shown in Fig. 3(a), on increasing the cavity height (H_1), ε_{eff} is reduced. Further, for cavity height of $H_1 = 0.250$ mm, ε_{eff} may even be reduced to the value of one. Fig. 3(b) shows the plot of normalized conductor width ($W_F/(H + t_1)$) vs ε_{eff} and characteristic impedance (Z_0) of the suspended microstrip line, for a fixed air cavity height $H_1 = 0.179$ mm corresponding to $\varepsilon_{eff} = 2.2$. From Fig. 3(b), it is clear that the highest impedance that can be achieved with this design is 120 Ω for V band (centre freq. = 60 GHz) and 140 Ω for W band (centre freq. = 94 GHz) for a microstrip width (W_F) variation of 0.1 mm to 1.5 mm. Suspended microstrip line width (W_F) = 0.75 mm gives around 50 Ω impedance in the mm-wave band (both V and W bands). Further, Fig. 3(c) shows a full variation of around 22% and 4% for ε_{eff} and Z_0 w.r.t. frequency (i.e., 1 GHz to 110 GHz) at fixed $W_F = 0.75$ mm and $H_1 = 0.179$ mm.

3.2. Dual Band Micromachined Antenna Results

The dual-band mm-wave antenna was designed over a bulk micromachined substrate with air cavity height $H_1 = 0.179$ mm corresponding to $\varepsilon_{eff} \approx 2.2$. The micromachined cavity dimensions ($L \times W_C \times H_1$) were 10 mm × 5 mm × 0.179 mm. Final optimized dimensions of the designed micromachined dual-band antenna are shown in Table 1.

Figure 4(a) shows the simulated return loss plot of the proposed mm-wave dual-band antenna showing two resonances at 60 GHz and 94 GHz, with a very good inter band rejection. The 10-dB bandwidths are 2.2 GHz (3.7%) and 4.5 GHz (5%) at 60 GHz and 94 GHz, respectively. Figs. 4(b) and

Table 1. Final micromachined dual band microstrip planar antenna dimensions.

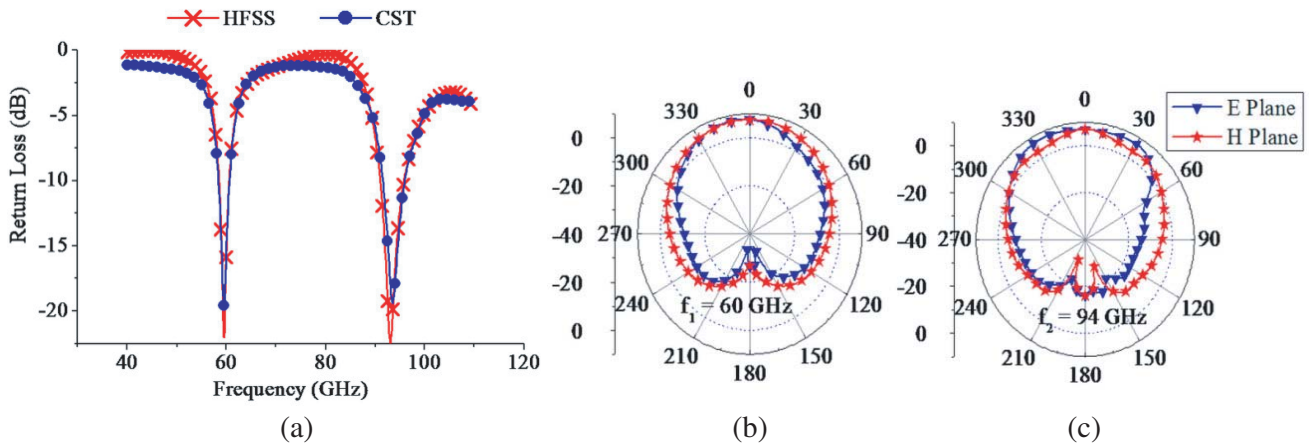| Parameter	L_P	W_P	L_Q	W_Q	L_S	W_S
Value (in mm)	0.92	1.6	0.87	0.35	0.5	0.8

(a)   (b)   (c)

Figure 4. Dual band mm-wave antenna (60 GHz/94 GHz) on micromachined silicon substrate. (a) Comparative simulated return loss plot, (b) radiation pattern plot at 60 GHz (E & H plane), (c) and 94 GHz (E & H plane).

4(c) show radiation patterns at 60 GHz and 94 GHz for both the E plane and H plane. At $f_1 = 60$ GHz, the pattern shows broadside radiation with the gain value of 7.68 dBi in both the E plane and H plane. Half power beamwidths (HPBWs) are 52° and 68° in E plane and H plane, respectively. At $f_2 = 94$ GHz, the pattern also shows the broadside radiation with the maximum gain of 8.22 dBi in both E plane and H plane; HPBWs are 44° and 62°, in E plane and H plane, respectively. Further, the designed dual-band antenna shows the nearly isotropic behaviour of radiation pattern.

Figure 5 shows the surface current distribution of radiating patch at the two frequencies. At $f_1 = 60$ GHz, surface current shows one half wavelength variation along the length of the patch. At $f_2 = 94$ GHz, current distribution shows one half wavelength variation along the length as well as the width of the patch.

Further, in view of stringent fabrication and measurement complexities at mm-wave frequency, a scaled prototype antenna model was fabricated and measured as a proof of concept (as discussed in
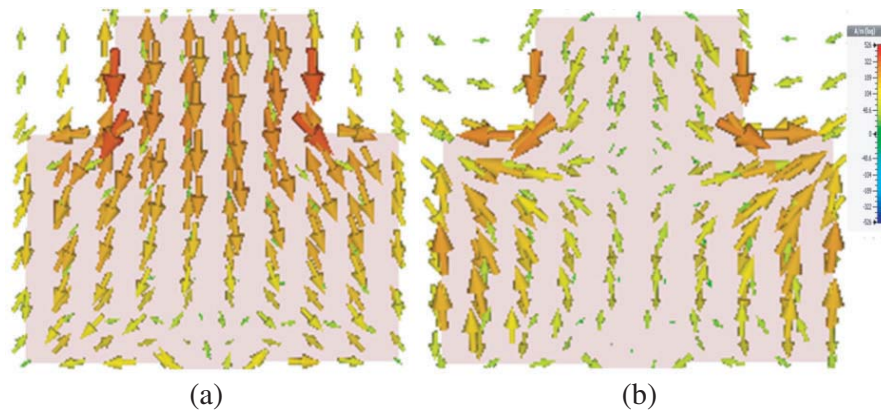

(a)   (b)

Figure 5. Surface Current distribution. (a) 60 GHz. (b) 94 GHz.

Section 4). Earlier, different researchers also used frequency scaled prototype approach for performance measurements at such high frequencies as per scaling principle [25–28].

3.3. Parametric Analysis of Substrate Parameters on Antenna Performance

Study of the effect of different substrate parameters, like substrate resistivity, substrate height, and air cavity height on antenna resonance behaviour, has also been done in order to completely analyze their effects on antenna performance. As shown in Fig. 6(a), when the resistivity of silicon wafer is varied from $5000\,\Omega$cm $(0.02\,\mathrm{S/m})$ to $5\,\Omega$cm $(20\,\mathrm{S/m})$, the losses are incurred because the increased conductivity causes degradation in antenna performance leading to reduction in gain from $7.68\,\mathrm{dBi}/8.22\,\mathrm{dBi}$ to $-3.3\,\mathrm{dBi}/-9.3\,\mathrm{dBi}$ at $60\,\mathrm{GHz}/94\,\mathrm{GHz}$, respectively. This, in turn, reduces antenna radiation efficiency significantly. This behaviour suggests that some special techniques like dielectric/polymide coating are needed to be employed if low resistive silicon wafer is used for antenna design.
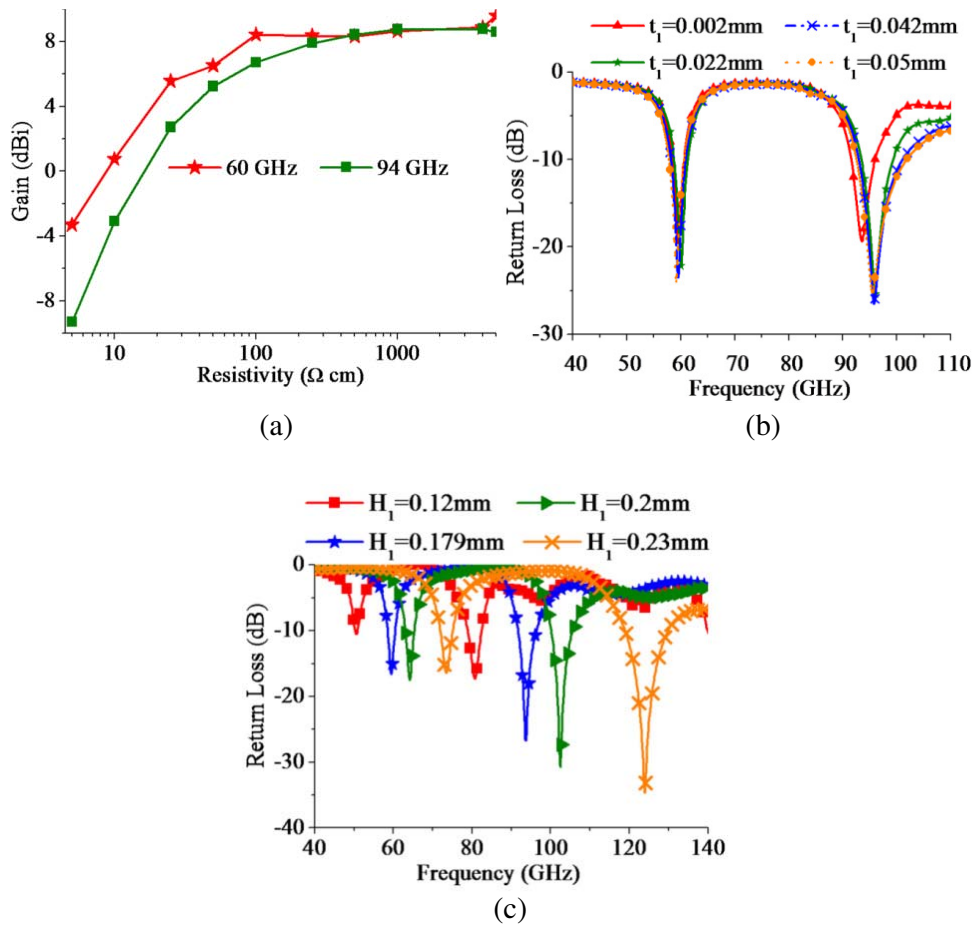

(a)   (b)

(c)

Figure 6. Effect on antenna performance *w.r.t.* variation in (a) resistivity of silicon wafer, (b) oxide thickness, (c) micromachined cavity height.

Figures 6(b), 6(c) show the effects of dielectric (SiO_2) thickness (t_1) and micromachined cavity height (H_1) on antenna resonance frequencies, respectively. With increasing SiO_2 thickness, there is a slight shift in frequency at higher frequency resonance points. However, with changing air cavity height (H_1), there is a large shift in the two bands, i.e., from $50/80\,\mathrm{GHz}$ to $73/124\,\mathrm{GHz}$, while increasing H_1 from $0.12\,\mathrm{mm}$ to $0.23\,\mathrm{mm}$. The parametric study suggests that high index Si substrate can also support good antenna performance by a careful choice of micromachining for the system on chip applications at mm-wave. This will facilitate the development of a compact, simple, and efficient RF system.

4. SCALED PROTOTYPE ANTENNA FABRICATION AND MEASUREMENT

Further, as a proof of concept, the performance of the micromachined silicon on-chip mm-wave antenna has been compared with a commercially available substrate (Arlon Cuclad 217LX) having relative permittivity ($\varepsilon_r = 2.2$) and height = 1.57 mm (62 mil) using frequency scaling technique [29, 30]. For scaled antenna design, the substrate attributes were taken in accordance with the scaling principle. Geometrical scale modelling by a factor of n requires the scaling as indicated in Table 2. The primed parameters represent the scaled prototype parameters.

Table 2. Geometrical scale modelling principle.

S. No.	Scaled Parameters		Unchanged Parameters	
	Parameter	Description	Parameter	Description
1	$L' = n \times L$	Geometrical dimension	$\varepsilon' = \varepsilon$	Permittivity
2	$f' = f/n$	Frequency	$\mu' = \mu$	Permeability
3	$\sigma' = \sigma/n$	Conductivity	$V' = V$	Velocity
4	$\lambda' = n \times \lambda$	Wavelength	$Z' = Z$	Impedance
5	$t' = t \times n$	Time	$G' = G$	Antenna Gain

As per scaling principle, the scaled prototype substrate should have relative permittivity equivalent to the effective permittivity of micromachined Si. Hence, the choice of a Teflon substrate fits well to satisfy this condition, i.e.,

$$\varepsilon_{r(\text{teflon})} \approx \varepsilon_{\textit{eff} \ (\text{micromachined Si})} = 2.2 \tag{2}$$

Likewise, the height of the Teflon substrate should be

$$H_{(\text{teflon})} \approx n \times H_{(\text{micromachined Si})} \tag{3}$$

where n = scaling factor.

Since $H_{(\text{teflon})} = 1.57$ mm, $H_{(\text{micromachined Si})}) = 0.254$ mm,

$$\text{Hence, this gives scaling factor } n = 1.57 \, \text{mm}/0.254 \, \text{mm} = 6.2 \tag{4}$$

Thus, the two mm-wave resonant frequencies will also scale down in proportion to scaling factor for design of analogues scaled dual-band antenna such that

$$(60 \, \text{GHz}/6.2) \sim \mathbf{9.67 \, GHz}; \ (94 \, \text{GHz}/6.2) \sim \mathbf{15.16 \, GHz} \tag{5}$$

Simultaneously all antenna design dimensions will be scaled up by the scaling factor $n = 6.2$ accordingly. The antenna prototype as per scaled dimensions was designed, simulated, and fabricated as a proof of concept to the proposed micromachined mm-wave dual-band antenna in view of available fabrication and testing facilities. Fig. 7(a) shows the fabricated scaled prototype and measurement setup.

Vector network analyzer (VNA) of Rohde & Schwarz ZVM (10 MHz–20 GHz) has been used for Scattering parameter (S_{11}) measurements of the fabricated antenna prototype. Before starting with the measurements, VNA was first calibrated with the standard short circuit, open circuit, and matched load (50 ohm) for the frequency range of interest, i.e., 1 GHz to 18 GHz in order to nullify the effects of cable and connector. Fig. 7(b) is the S-parameter plot showing dual resonances at the two respective scaled frequencies along with the comparison of two different EM solvers HFSS, CST with the measurement results. As seen, the three results are in close agreement. At the two resonant frequencies $f'_1 = 9.6$ GHz and $f'_2 = 15.2$ GHz of the scaled prototype, the fractional bandwidths (FBWs) are 3.8% (0.37 GHz) and 6.6% (1 GHz), and the gains are 7.4 dBi and 6.8 dBi, respectively.

The radiation pattern of the fabricated antenna was measured in a well equipped anechoic chamber using a standard horn antenna as the reference antenna. The AUT (antenna under test) was used as a receiving antenna and horn antenna used as a transmitting antenna. The power received by AUT was
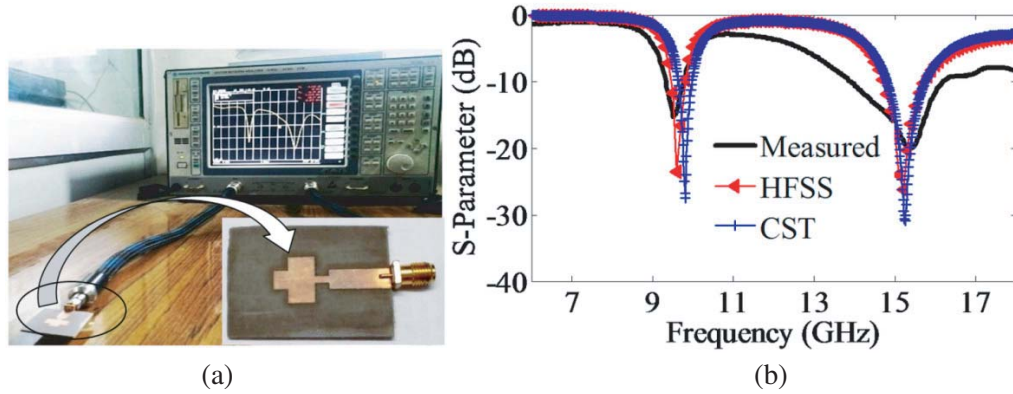
(a)   (b)

Figure 7. (a) Measurement setup and fabricated prototype. (b) Comparative S-parameter plot of scaled prototype antenna.

(a)   (b)
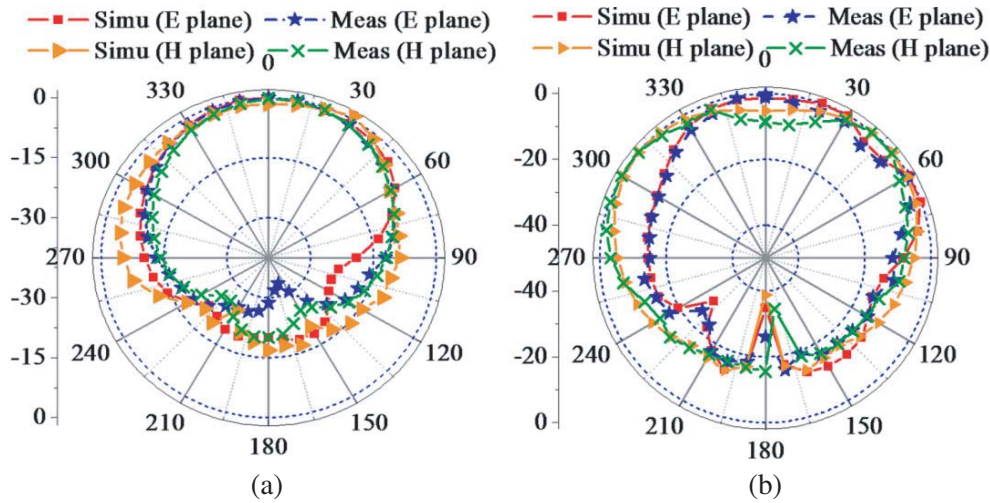
Figure 8. Comparative radiation pattern plots (simulated *vs* measured) of fabricated scaled prototype dual band antenna. (a) 9.6 GHz. (b) 15.2 GHz.

Table 3. Antenna performance parameters comparison.

	Resonant frequencies (GHz)	Fractional Bandwidth (%)	Gain (dBi)	Radiation Pattern
Proposed mm-wave antenna	60, 94	3.7, 5	7.68, 8.22	Broadside
Scaled prototype antenna	9.6, 15.2	3.8, 6.6	7.9, 7.58	Broadside

measured at every step increment of theta angle (elevation angle) from $-180°$ to $180°$ (in steps of $5°$) for E-plane (azimuth angle, phi = $0°$) and H-plane (azimuth angle, phi = $90°$) at frequencies 9.6 GHz and 15.2 GHz. The radiation patterns thus obtained were drawn in polar plot form as shown in Fig. 8(a) for 9.6 GHz and in Fig. 8(b) for 15.2 GHz in both E and H planes. The measured radiation patterns were also compared with simulated ones. The radiation plots show broadside radiation which is analogues to the proposed mm-wave antenna.

Table 3 shows the comparison of antenna performance measurements *viz.* dual resonant frequencies, fractional bandwidths, radiation patterns, antenna gains of the proposed micromachined mm-wave

Table 4. Comparison of the proposed mm-wave dual band antenna with the existing literature.

S. No.	Ref.	[11]	[17]	[13]	[19]	[18]	This work
1	**Freq (GHz)**	135	27.2	29.5	41/52.2	60/77	**60/94**
2	**Dual bands**	No	No	No	Yes (Dual SRRs)	Yes (moveable buckled cantilever)	**Yes (Open circuited stub)**
3	**Substrate**	Si	Si	Si	LTCC	Si	**Si**
4	**Technique**	micro-machining	air-elevated	micro-machining	meta-resonator	MEMS	**micro-machining**
5	**Feed**	CPW	CPW	CPW	microstrip	CPS	**microstrip**
6	**Antenna Design**	Triangular monopole	Rect. patch	slot loop antenna	SRR	fractal Bowtie	**Rect. patch**
7	**BW (%)**	9/-	10.5/-	-	2/-	-	**3.7/5**
8	**Gain (dBi)**	6.74/-	9.5/-	1.5/-	3.8/4.2	3.5/4.8	**7.7/8.2**
9	**Complexity**	moderate	complex	moderate	complex	complex	**simple**
10	**Size (mm^2)**	-	5.8×4.8	3.6×3.6	-	2×2.3	**1.6×1.42**

antenna and the analogues scaled prototype antenna which validates the results in accordance with the scaling principle. In addition, wider bandwidth and better antenna gain achieved over high index Si wafer suggest the use of bulk micromachining technique at mm-wave frequencies for compact, light-weight system on-chip applications. Further, the simple design and dual-band support makes the proposed structure a strong solution for emerging concurrent applications, like high data rate wireless communication and high resolution standoff imaging at 60 GHz and 94 GHz, respectively. Table 4 shows the comparison of the proposed work with similar reported literature at mm-wave frequencies.

5. CONCLUSION

A Si bulk micromachined dual-band mm-wave antenna operating concurrently at 60 GHz and 94 GHz has been designed, and the performance of antenna has been analysed for different substrate parameters for system on-chip applications. The results were also compared using two different EM solvers HFSS and CST which strongly matched. The proposed mm-wave antenna shows fractional bandwidths of 3.7% & 5% and has gains of 7.68 dBi & 8.22 dBi at 60 GHz and 94 GHz, respectively. The urgent need of maximizing data rate, minimizing operational cost, size, and increasing compatibility of RF front end for system integration are the key outlines of the proposed approach. Bulk micromachining technique provides easy and improved system integration enabling single chip RF front end at mm-wave frequency. Further, results suggest that by carefully adjusting the micromachined cavity height, specific antenna resonance frequencies can be achieved for MMIC applications, i.e., 0.179 mm air cavity is corresponding to 60 & 94 GHz frequencies. The dual resonances simultaneously support two promising applications, multi-gigabit wireless link (60 GHz) and high-resolution standoff imaging (94 GHz). Further, scaled prototype antenna measurement results have been presented as a proof of concept which validates the proposed mm-wave dual-band antenna results. Moreover, the proposed design is simple, fabrication friendly, compact, and easily integrable for MMIC applications.

REFERENCES

1. Zhang, Y. and J. Mao, "An overview of the development of antenna-in-package technology for highly integrated wireless devices," *Proceedings of the IEEE*, 2019.

2. Anab, M., M. I. Khattak, S. M. Owais, A. Ali Khattak, and A. Sultan, "Design and analysis of millimeter wave dielectric resonator antenna for 5G wireless communication systems," *Progress In Electromagnetics Research C*, Vol. 98, 239–255, 2020.

3. Alavi, S., et al., "Towards 5G: A photonic based millimeter wave signal generation for applying in 5G access fronthaul," *Scientific Reports*, Vol. 6, 19891, 2016.

4. Al-Shareefi, N. A., S. I. S. Hassan, M. F. B. A. Malek, R. Ngah, S. A. Abbas, and S. A. Aljunid, "A cost-effective method for high-quality 60 GHz optical millimeter wave signal generation based on frequency quadrupling," *Progress In Electromagnetics Research*, Vol. 137, 255–274, 2013.

5. Liu, C., M.-H. Yang, and X.-W. Sun, "Towards robust human millimeter wave imaging inspection system in real time with deep learning," *Progress In Electromagnetics Research*, Vol. 161, 87–100, 2018.

6. Agarwal, S., D. Singh, and N. P. Pathak, "Active millimeter wave radar system for non-destructive, non-invasive underline fault detection and multilayer material analysis," *2014 IEEE International Microwave and RF Conference (IMaRC)*, 2014.

7. Mosalanejad, M., S. Brebels, C. Soens, I. Ocket, and G. A. E. Vandenbosch, "Millimeter wave cavity backed microstrip antenna array for 79 GHz radar applications," *Progress In Electromagnetics Research*, Vol. 158, 89–98, 2017.

8. Jackson, D. R., et al., "Microstrip patch designs that do not excite surface waves," *IEEE Transactions on Antennas and Propagation*, Vol. 41, No. 8, 1026–1037, 1993.

9. Gauthier, G. P., et al., "A 94-GHz aperture-coupled micromachined microstrip antenna," *IEEE Transactions on Antennas and Propagation*, Vol. 47, No. 12, 1761–1766, 1999.

10. Papapolymerou, I., R. F. Drayton, and L. P. Katehi, "Micromachined patch antennas," *IEEE Transactions on Antennas and Propagation*, Vol. 46, No. 2, 275–283, 1998.

11. Chu, H., et al., "135-GHz micromachined on-chip antenna and antenna array," *IEEE Transactions on Antennas and Propagation*, Vol. 60, No. 10, 4582–4588, 2012.

12. Yook, J.-G. and L. P. Katehi, "Micromachined microstrip patch antenna with controlled mutual coupling and surface waves," *IEEE Transactions on Antennas and Propagation*, Vol. 49, No. 9, 1282–1289, 2001.

13. Ojefors, E., et al., "Micromachined loop antennas on low resistivity silicon substrates," *IEEE Transactions on Antennas and Propagation*, Vol. 54, No. 12, 3593–3601, 2006.

14. Vaughan, M. J., K. Y. Hur, and R. C. Compton, "Improvement of microstrip patch antenna radiation patterns," *IEEE Transactions on Antennas and Propagation*, Vol. 42, No. 6, 882–885, 1994.

15. Gauthier, G. P., A. Courtay, and G. M. Rebeiz, "Microstrip antennas on synthesized low dielectric-constant substrates," *IEEE Transactions on Antennas and Propagation*, Vol. 45, No. 8, 1310–1314, 1997.

16. Yang, H.-Y., N. G. Alexopoulos, and E. Yablonovitch, "Photonic band-gap materials for high-gain printed circuit antennas," *IEEE Transactions on Antennas and Propagation*, Vol. 45, No. 1, 185–187, 1997.

17. Pan, B., et al., "Analysis and characterization of a high-performance Ka-band surface micromachined elevated patch antenna," *IEEE Antennas and Wireless Propagation Letters*, Vol. 5, 511–514, 2006.

18. Marnat, L., et al., "New movable plate for efficient millimeter wave vertical on-chip antenna," *IEEE Transactions on Antennas and Propagation*, Vol. 61, No. 4, 1608–1615, 2013.

19. Kim, I. K. and V. V. Varadan, "Electrically small, millimeter wave dual band meta-resonator antennas," *IEEE Transactions on Antennas and Propagation*, Vol. 58, No. 11, 3458–3463, 2010.

20. Huang, J.-H., et al., "A 24/60 GHz dual-band millimeter-wave on-chip monopole antenna fabricated with a 0.13-µm CMOS technology," *2009 IEEE International Workshop on Antenna Technology*, IEEE, 2009.

21. Katehi, L. P., J. F. Harvey, and E. Brown, "MEMS and Si micromachined circuits for high-frequency applications," *IEEE Transactions on Microwave Theory and Techniques*, Vol. 50, No. 3, 858–866, 2002.

22. Maci, S. and G. B. Gentili, "Dual-frequency patch antennas," *IEEE Antennas and Propagation Magazine*, Vol. 39, No. 6, 13–20, 1997.

23. Pozar, D. M., *Microwave Engineering*, John Wiley & Sons, 2009.

24. Sharma, P. and S. K. Koul, "Design and development of millimeter-wave micromachined patch antennas," *IETE Journal of Research*, Vol. 55, No. 1, 40–50, 2009.

25. Hsu, Y.-C., K.-H. Lin, and Y.-C. Huang, "A scale-sized model for analysis of vehicular antennas," *2007 IEEE Antennas and Propagation Society International Symposium*, IEEE, 2007.

26. Hesler, J. L., et al., "Analysis of an octagonal micromachined horn antenna for submillimeter-wave applications," *IEEE Transactions on Antennas and Propagation*, Vol. 49, No. 6, 997–1001, 2001.

27. Eckart, A., A. Harris, and R. Wohlleben, "Scaled model measurements of the sandwiched V-antenna," *International Journal of Infrared and Millimeter Waves*, Vol. 9, No. 6, 505–520, 1988.

28. Hasch, J., et al., "Patch antenna on micromachined silicon," *Silicon Monolithic Integrated Circuits in RF Systems*, 2004.

29. Chiappe, M. and G. L. Gragnani, "Vivaldi antennas for microwave imaging: Theoretical analysis and design considerations," *IEEE Transactions on Instrumentation and Measurement*, Vol. 55, No. 6, 1885–1891, 2006.

30. Sinclair, G., "Theory of models of electromagnetic systems," *Proceedings of the IRE*, Vol. 36, No. 11, 1364–1370, 1948.